Hybrid Cu_xO/TiO_2 Nanocomposites As Risk-Reduction Materials in Indoor Environments

Xiaoqing Qiu,[‡] Masahiro Miyauchi,[†,*] Kayano Sunada,[‡] Masafumi Minoshima,[⊥] Min Liu,[‡] Yue Lu,[⊥] Ding Li,[§] Yoshiki Shimodaira,[∥] Yasuhiro Hosogi,[§] Yasushi Kuroda,[§] and Kazuhito Hashimoto[‡,⊥,*]

[†]Department of Metallurgy and Ceramics Science, Graduate School of Science and Engineering, Tokyo Institute of Technology, 2-12-1 Ookayama, Meguro-ku, Tokyo 152-8552, Japan, [‡]Research Center for Advanced Science and Technology, The University of Tokyo, 4-6-1 Komaba, Meguro-ku, Tokyo 153-8904, Japan, [§]Showa Titanium Co., Ltd, 3-1 Nishinomiya-machi, Toyama, Toyama 931-8577, Japan, [∥]Corporate R&D Center, Showa Denko K. K., 1-1-1 Ohnodai, Midori-ku, Chiba, Chiba, 267-0056, Japan, and [⊥]Graduate School of Engineering, The University of Tokyo, 7-3-1 Hongo, Bunkyo-ku, Tokyo 113-8656, Japan

ABSTRACT

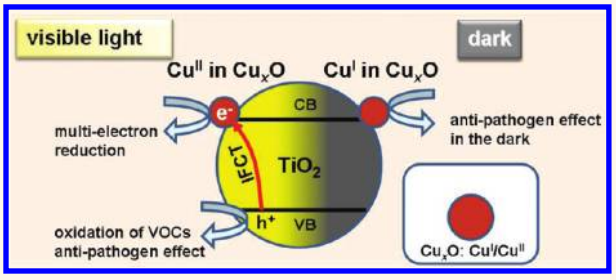

Photocatalytic TiO_2 powders impart ultraviolet light-induced self-cleaning and antibacterial functions when coated on outdoor building materials. For indoor applications, however, TiO_2 must be modified for visible-light and dark sensitivity. Here we report that the grafting of nanometer-sized Cu_xO clusters onto TiO_2 generates an excellent risk-reduction material in indoor environments. X-ray absorption near-edge structure using synchrotron radiation and high-resolution transmission electron microscopic analyses revealed that Cu_xO clusters were composed of Cu^I and Cu^{II} valence states. The Cu^{II} species in the Cu_xO clusters endow TiO_2 with efficient visible-light photooxidation of volatile organic compounds, whereas the Cu^I species impart antimicrobial properties under dark conditions. By controlling the balance between Cu^I and Cu^{II} in Cu_xO, efficient decomposition and antipathogenic activity were achieved in the hybrid Cu_xO/TiO_2 nanocomposites.

KEYWORDS: TiO_2 · multifunction · volatile organic compounds · photocatalysis · antipathogen · indoor environment

Indoor air quality is an important determinant of population health and well being.[1,2] One of the sources of indoor air pollution is volatile organic compounds (VOCs), which originate from various sources and are the major cause of sick house syndrome.[3] In addition to VOCs, exposure to infectious pathogens (bacteria and virus) with multiple-drug resistance often occurs in our daily environment and can adversely impact health.[4,5] Photocatalytic oxidation over semiconductors is regarded as a promising approach for environmental remediation. Among the various photocatalysts, titanium dioxide (TiO_2) photocatalyst possesses air purification and/or antibacterial functions, but it is only activated by ultraviolet (UV) irradiation with strong light intensity, such as sunlight or black light fluorescent bulbs.[6−8] However, the UV intensity from typical indoor lighting sources, such as white light fluorescent bulbs, is below several $\mu W/cm^2$, an intensity that is one thousand times lower than that of sunlight.[9] Other indoor lighting sources, such as white incandescent lamps or white-light emission diodes (LEDs), do not emit UV light. Therefore, the development of visible-light-sensitive photocatalysts is necessary for applications in indoor environments.

Over the past 30 years, many researchers have attempted to develop visible-light-sensitive photocatalysts through the doping of TiO_2 with transition metal ions[10−12] or anions.[13−15] Despite extensive investigations, most developed systems are not suitable for practical indoor applications because of the low light-harvesting efficiency of the resulting carrier recombination centers in metal-ion-doped TiO_2[10,16] or the low oxidation power and mobility of the photogenerated holes in non-metal-doped TiO_2.[17] In addition to visible-light sensitivity, performance sustainability of a photocatalyst under dark conditions is also critical for practical applications. The surfaces of TiO_2 have been modified with robust functional materials, including silver and porous inorganic adsorbents, to achieve antibacterial and air purification properties even in dark conditions.[18] Notably, the antiviral effects of modification with solid inorganic materials have not been studied comprehensively for

* Address correspondence to mmiyauchi@ceram.titech.ac.jp, hashimoto@light.t.u-tokyo.ac.jp.

Received for review November 25, 2011 and accepted December 30, 2011.

Published online December 30, 2011
10.1021/nn2045888

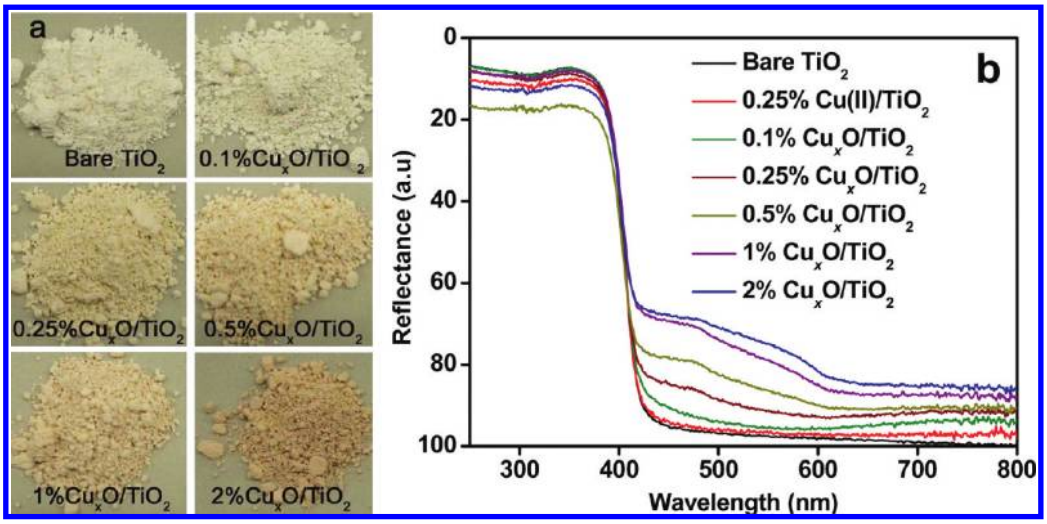

Figure 1. (a) Photos of the prepared Cu_xO/TiO_2 nanocomposites showing the color evolution with increasing Cu content. (b) UV−visible reflectance spectra of TiO_2, Cu(II)/TiO_2 (*i.e.*, TiO_2 modified with Cu(II) ions), and the Cu_xO/TiO_2 nanocomposites.

TiO_2-based photocatalysts, although the antiviral effects of organic molecules have been investigated in medicine or vaccination. Antiviral organic molecules, however, are not appropriate to combine with TiO_2 because they are easily degraded during the photocatalytic process. So far no route is available for fabricating such active risk-reduction materials that can both eliminate the VOCs under visible-light irradiation and inactivate the pathogens under indoor conditions.

In the present study, we set the following requirements for developing a risk-reduction material for use in indoor environments: (i) robust inorganic materials composed of nontoxic and naturally abundant elements; (ii) visible-light activity with strong oxidation power; and (iii) antipathogenic (antibacterial and antiviral) effects, even in dark conditions. Barreca *et al.* have reported the overdispersion of TiO_2 nanoparticles on copper oxide matrixes by a vapor phase approach and demonstrated the promising applications of the as-obtained nanocomposites in photoactivated H_2 generation and in gas sensing of toxic/flammable pollutants.[19−22] Our recent investigation on the antiviral effects of various solid-state materials revealed that copper compounds with Cu^I species (CuI, Cu_2S, or Cu_2O) were effective on both the antibacterial and antiviral properties, even under dark conditions.[23] On the basis of these results combined with our previous findings of the beneficial effects of Cu^{II} species on the photooxidation of VOCs,[24−28] we anticipated that TiO_2 grafted with nanoclusters containing Cu^I and Cu^{II} species might be effective as a risk-reduction material for indoor applications. In particular, the most attractive advantages of our Cu_xO/TiO_2 nanocomposites may lie in public health applications.

RESULTS AND DISCUSSION

The hybrid Cu_xO/TiO_2 nanocomposites used in this study were prepared using a simple impregnation method.[27] Briefly, commercial rutile TiO_2 with preannealing treatment was used as the starting material and was dispersed into a $CuCl_2$ solution in a vial reactor. Then NaOH and glucose solutions were added to reduce Cu^{II} to Cu^I at 90 °C and control the Cu^I/Cu^{II} ratio in the final products. The total amount of Cu in the prepared samples was determined using inductively coupled plasma atomic emission spectrometry and was found to be nearly equal to the initial concentration used in the preparation. The color of the as-obtained samples changed from white to slightly yellow and slightly red with increasing content of Cu_xO (Figure 1a). Diffuse reflectance spectroscopy clearly indicated that the optical absorbance properties in the visible-light region were markedly enhanced in the prepared nanocomposite samples compared to TiO_2 (Figure 1b and Figure S1 in the Supporting Information). Besides the intrinsic interband absorption at 400 nm of TiO_2, the hybrid Cu_xO/TiO_2 nanocomposites showed three additional absorption bands. The absorption in the range 800−600 nm is attributable to the intrinsic exciton band of CuO and the d−d transition of Cu^{II} species.[29] The absorption band in the range 600−500 nm is due to the interband absorption of Cu_2O,[30] and the weak absorption from 500 to 400 nm originates from the interfacial charge transfer (IFCT) from the valence band of TiO_2 to the Cu_xO clusters.[24] As shown in Figure 2, strong X-ray diffraction (XRD) peaks were also observed, demonstrating the high crystallinity of the rutile structure present in the samples. When the content of Cu was below 1%, no peaks associated with Cu metal, Cu_2O, CuO, or $Cu(OH)_2$ were detected in the XRD patterns. This result was likely due to the low crystallinity and the high dispersion of Cu_xO on TiO_2 surfaces. When the Cu content in the nanocomposite exceeded 1%, diffraction peaks of Cu_2O were clearly observed in the XRD patterns (Figure 2, left frame), indicating the existence of Cu^I species in the samples.

X-ray photoelectron spectroscopy (XPS) was employed to explore the chemical states of surface elements of the nanocomposite samples. Two well-resolved peaks at 463.9 and 458.2 eV were observed from the Ti 2p core-level spectrum (Figure 3a), which can be assigned to Ti $2p_{1/2}$ and Ti $2p_{3/2}$ spin−orbital components in TiO_2, respectively.[31] Obviously, no distinct difference was observed between the two spectra of bare TiO_2 and 0.25% Cu_xO/TiO_2, indicating that Cu_xO deposited on the surfaces of TiO_2 rather than the lattice doping. As illustrated in the Cu 2p core-level spectrum (Figure 3b), both Cu^I and Cu^{II} species were present in the as-obtained Cu_xO/TiO_2 samples.[32] However, it should be noted that the Cu(II)/TiO_2 samples, the unitary Cu^{II} nanocluster-grafted TiO_2, showed the Cu 2p transitions of Cu^I species. This is because the Cu 2p transitions of Cu^{II} species shift to lower binding energies and overlap with the signal of Cu^I species, resulting from the bombardment effect by X-ray irradiation under high vacuum, when Cu content is very low and exists in a highly dispersed state on the TiO_2 surfaces (Figure S2 in the Supporting Information).[33]

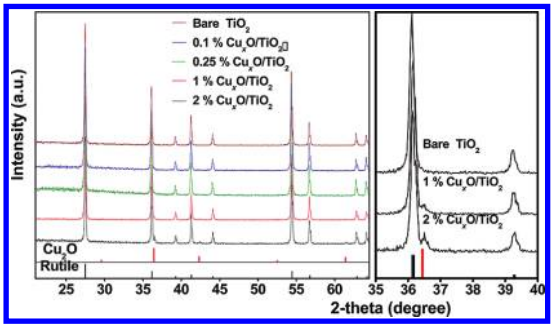

Figure 2. XRD patterns of the Cu_xO/TiO_2 nanocomposites. Cu_2O peaks were observed when the Cu content was 1% or greater, as shown in the enlarged pattern on the right.

For this reason, we could not determine the actual Cu^I/Cu^{II} ratios in the samples based on the XPS analysis.

To further investigate the Cu state in the samples, we performed quantitative measurements using X-ray absorption near-edge structure (XANES), which is a powerful tool to determine the state of electrons in materials.[34] We conducted XANES analysis of the Cu_xO/TiO_2 nanocomposite in air using the synchrotron apparatus of the SPring-8 facility. For Cu(II)/TiO_2 (*i.e.*, TiO_2 modified with Cu(II) ions), the chemical environment of Cu^{II} species resembled that of $Cu(OH)_2$, suggesting that the Cu^{II} species was attached on the surfaces, forming a distorted five-coordinate square-pyramidal structure with −O, −OH, or $-OH_2$ (Figure S3 in the Supporting Information).[28] As can be seen in Figure 4a, the Cu K-absorption edge of Cu_xO/TiO_2 was located between those of Cu_2O and $Cu(OH)_2$, indicating that the grafted Cu species resemble the chemical environment of Cu^I and Cu^{II} compounds. Thus, commercial Cu_2O and $Cu(OH)_2$ were used as standards for determining the relative proportion of the Cu^I and Cu^{II} states. As displayed in Figure 4b, peak I at 8982 eV is the diagnostic feature of Cu_2O, while peak II contains the information of both Cu^{II} and Cu^I.[35] Using the diagnostic peaks of Cu^I and Cu^{II} species, we calculated the ratio of Cu^I/Cu^{II} and found that it could be well controlled by adjusting the concentration of NaOH during the preparation process (Figure S3 in the Supporting Information). For 0.25% Cu_xO/TiO_2 nanocomposites displayed in Figure 4a, the ratio of Cu^I/Cu^{II} was thus determined to be 1.3. Transmission electron microscopy (TEM) analysis revealed that clusters of Cu_xO were well dispersed on the surfaces of TiO_2 (Figure 4c). We also performed energy dispersive X-ray spectroscopy (EDXS) point analysis using the TEM apparatus, which revealed that the small particles (5 nm) were composed of Cu

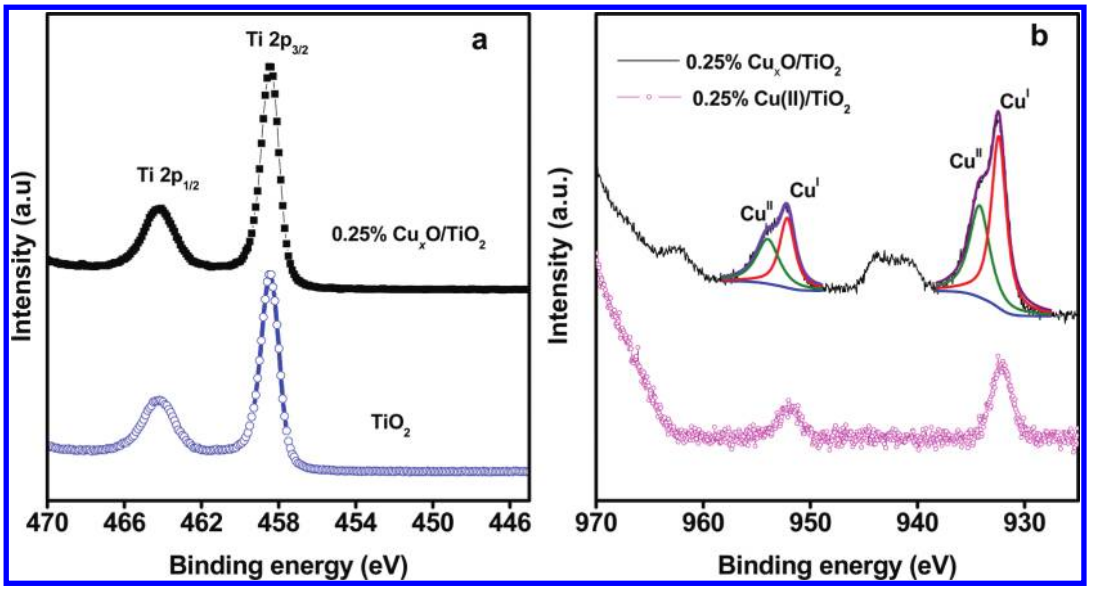

Figure 3. (a) Ti 2p core-level spectra of bare TiO_2 and 0.25% Cu_xO/TiO_2. (b) Cu 2p core-level spectra of 0.25% Cu(II)/TiO_2 and 0.25% Cu_xO/TiO_2.

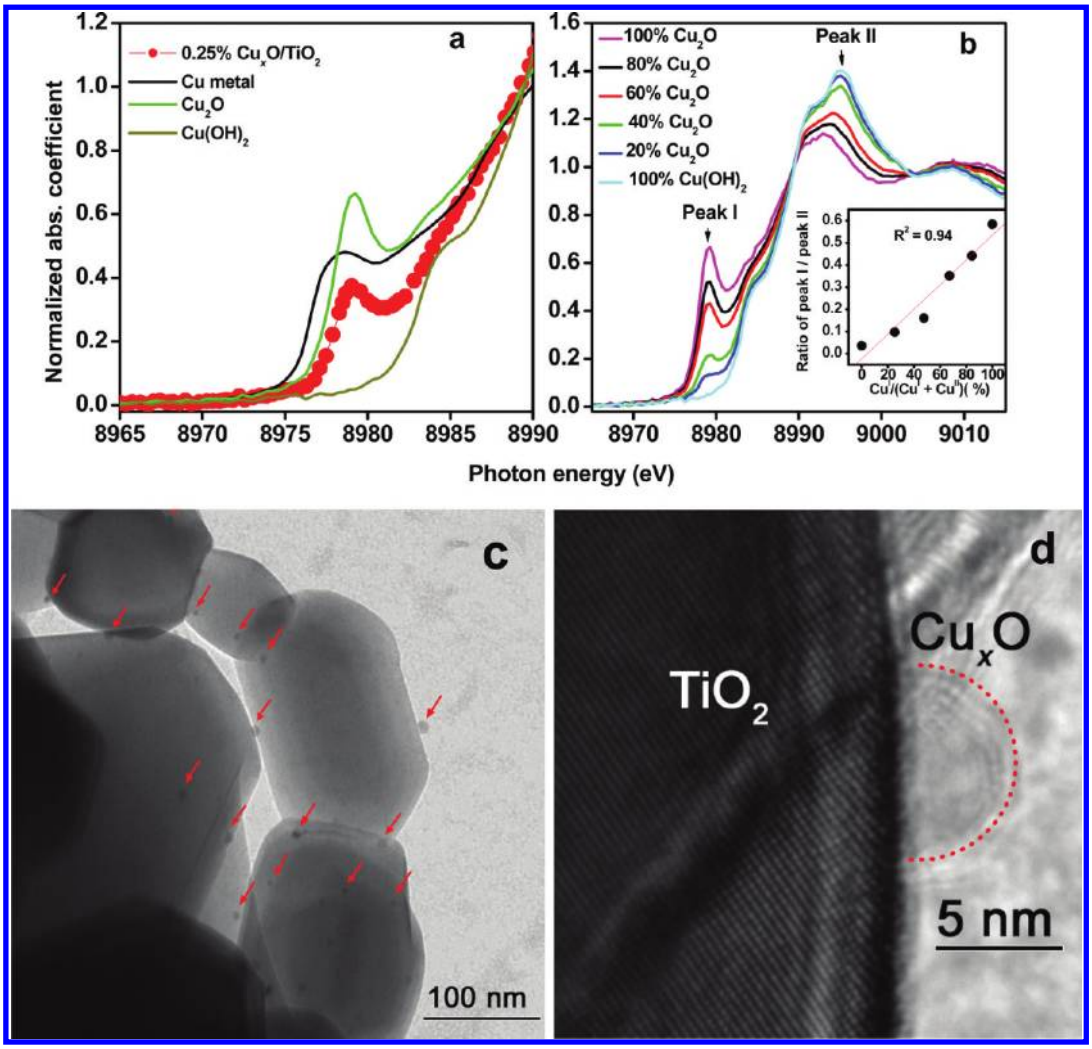

Figure 4. (a) Cu K-edge XANES spectra of Cu metal, Cu_2O, $Cu(OH)_2$, and as-prepared 0.25% Cu_xO/TiO_2 nanocomposites. The absorption edges correspond to 1 → 4p transition. (b) Cu K-edge XANES spectra of the mixture of Cu_2O and $Cu(OH)_2$. The inset of (b) displays a good linear relationship between Cu^I content and the ratio of peak I/peak II. (c and d) TEM and HR-TEM images of the 0.25% Cu_xO/TiO_2 (Cu^I/Cu^{II} = 1.3) sample. Cu_xO clusters (marked by red arrows) were highly dispersed on the TiO_2 surfaces. In (d), a Cu_xO particle is outlined by a dashed line. The good attachment of Cu_xO to TiO_2 can be clearly observed.

(Figure S4 in the Supporting Information). High-resolution TEM images showed that the Cu_xO clusters were attached onto the highly crystallized TiO_2 surfaces and formed clear lattice fringes (Figure 4d).

We evaluated the photocatalytic decomposition of VOCs over our samples under visible-light irradiation. Isopropyl alcohol (IPA) was used as a representative indicator of VOCs because it was reported as a serious pollutant of indoor air[36] and its oxidation pathway for CO_2 generation and the determination of quantum efficiency were comprehensively established in a previous study.[37] Considering the target application of the photocatalyst for indoor air purification, the light intensity was set to 1 mW/cm^2 and the wavelength of irradiation light ranged from 400 to 530 nm (Figure S5 in the Supporting Information). The selected visible-light intensity corresponds to an illuminance of only 300 lx, which is comparable to those of white fluorescent lights and white LED lights. For the performance tests, the initial concentration of IPA was set to 300 ppm, which is much higher than the actual VOC concentrations typically encountered in indoor environments. Ohko *et al.* reported the reaction pathway for VOC molecules by photocatalysis. It was found that VOC molecules such as IPA or acetaldehyde are completely decomposed to CO_2 and water by photocatalytic oxidation.[37] Figure 5a shows the typical change of the gas concentration during the process of the decomposition of IPA over the 0.25% Cu_xO/TiO_2 (Cu^I/Cu^{II} = 1.3) sample. Prior to light irradiation, the vessel was kept in the dark. The IPA concentration first decreased and then remained constant, suggesting the absorption/desorption equilibrium of IPA on the surfaces of materials. However, the acetone and CO_2 were not detected under dark conditions. This means that the IPA molecules were not decomposed by our Cu_xO/TiO_2 under dark conditions. With the visible-light irradiation, IPA concentration further decreased rapidly.

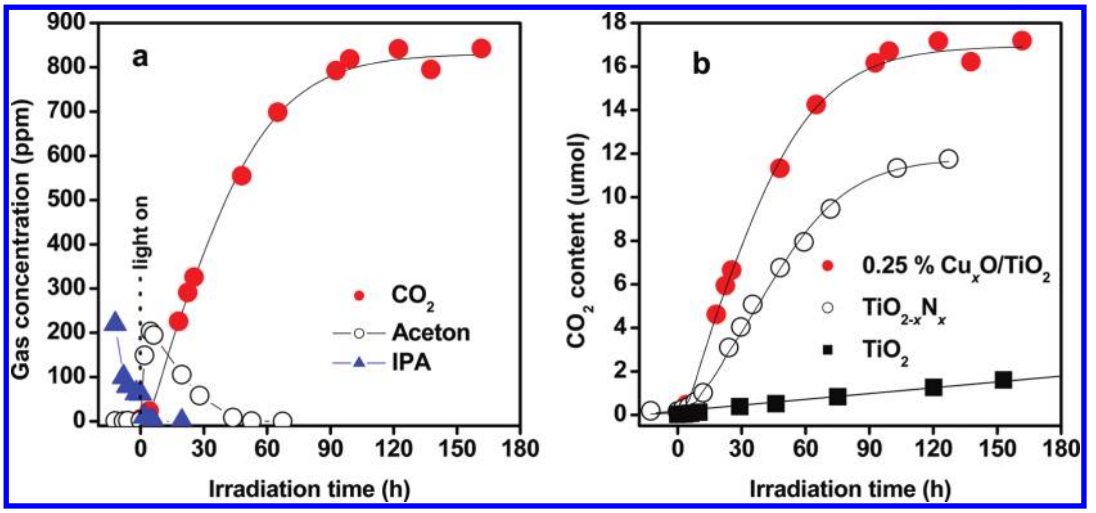

Figure 5. (a) Representative time-dependent gas concentrations during IPA decomposition over 0.25% Cu_xO/TiO_2 (Cu^I/Cu^{II} = 1.3) sample under visible-light irradiation. (b) Comparative studies of CO_2 generation over bare TiO_2, $TiO_{2-x}N_x$, and 0.25% Cu_xO/TiO_2 (Cu^I/Cu^{II} = 1.3) samples under the same conditions.

Meanwhile, the amount of acetone increased sharply. Accompanying the decease of acetone, the amount of CO_2 started to increase quickly. After 96 h of irradiation, the concentration of CO_2 reached approximately 900 ppm (*ca.* ~18 μmol), which was nearly 3 times the initially injected IPA, indicating the complete decomposition of IPA ($CH_3CHOHCH_3 + 9/2\ O_2 \rightarrow 3CO_2 + 4H_2O$). Figure 5b gives the comparative studies of photocatalytic activities of bare TiO_2, $TiO_{2-x}N_x$, and our Cu_xO/TiO_2 samples under the same conditions. CO_2 generation over bare TiO_2 was negligible under visible-light irradiation due to its wide band gap. The sample of $TiO_{2-x}N_x$, which has been recognized as one of the most efficient visible-light photocatalysts,[13] could not completely decompose gaseous IPA because of its low oxidation power,[17] indicating that intermediate molecules of IPA remained on the $TiO_{2-x}N_x$ surface. Thus, the long-term performance of the $TiO_{2-x}N_x$ photocatalyst for air purification cannot be expected. As can be seen in Figure 5b, the photocatalytic activity of the Cu_xO/TiO_2 sample was markedly superior to that of the $TiO_{2-x}N_x$ sample. The calculated quantum efficiencies of the Cu_xO/TiO_2 (Cu^I/Cu^{II} = 1.3) and $TiO_{2-x}N_x$ samples were 14.8% and 3.9%, respectively (Table S1 in the Supporting Information). Further, the visible-light activity of Cu_xO/TiO_2 was better than that of TiO_2 modified with Cu(II) ions (*i.e.*, the Cu(II)/TiO_2 samples), which was reported in our previous work (Figure S6 in the Supporting Information).[24,28] It is known that Cu_2O has a narrow band gap of about 2 eV.[30] To exclude the effect of excitation of Cu_2O, we grafted Cu_xO nanoclusters on a nonphotoactive SiO_2 and found the as-obtained Cu_xO/SiO_2 exhibited a negligible photoactivity to decompose IPA. We also investigated the visible-light activities of TiO_2 mixed with commercial Cu_2O particles (500 nm, ~5 μm grain size; Wako Chemical Co., Ltd.), but the activity of these samples was negligible under visible light (Figure S7 in the Supporting Information), indicating that the crystalline Cu_2O was photocatalytically inactive. In our hybrid Cu_xO/TiO_2 nanocomposites, Cu^{II} species in nanoclusters are very effective for the visible-light photocatalytic activity of TiO_2. When the Cu^{II} species are grafted on the surface of TiO_2, electrons in the valence band of TiO_2 are excited to Cu^{II} species in nanoclusters through an IFCT process.[24] The excited electrons effectively reduce atmospheric oxygen molecules through a multielectron reduction process, while holes in the valence band decompose organic substances due to their strong oxidation power.[27] It was noteworthy that the quantum efficiency of the Cu_xO/TiO_2 is very high, whereas IFCT absorption is small (Figure 1b). In the case of semiconductor bulk photocatalysts, photogenerated electrons and holes should migrate to the surface of the semiconductor. In our system, however, visible-light-induced excitation generates electrons to the surface nanoclusters with high reactive sites for oxygen reduction, resulting in high photocatalytic performance of our Cu_xO/TiO_2 system. In addition to IPA decomposition, our Cu_xO/TiO_2 nanocomposite was able to completely mineralize several other examined VOC molecules, including acetaldehyde, under visible-light irradiation (Figure S8 in the Supporting Information). The good stability of the Cu_xO/TiO_2 sample under long-term light irradiation was also confirmed by XAFS analysis (Figure S9 in the Supporting Information).

The inactivation of pathogenic microorganisms was next evaluated using thin film samples, which were prepared by coating suspensions of Cu_xO/TiO_2 on glass substrates. We used bacteriophage Qβ as a model of human influenza virus. The antiviral activities of our nanocomposite were tested by plaque assay according to the standard evaluation method of a photocatalytic

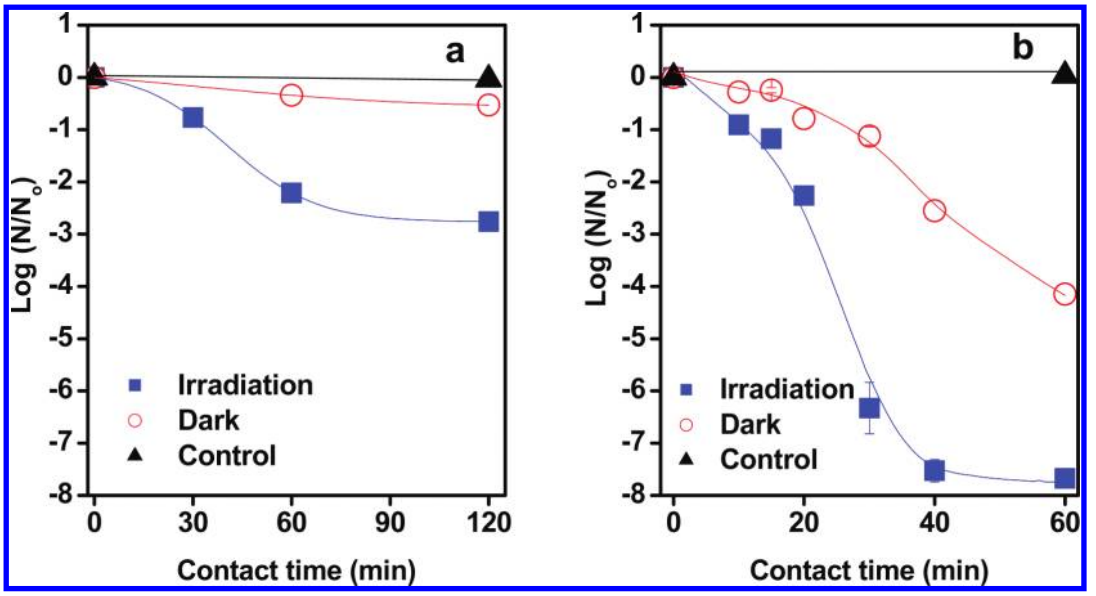

Figure 6. Inactivation of Qβ bacteriophage by the various samples under dark and visible-light irradiation. (a) 0.25% Cu(II)/TiO_2. (b) 0.25% Cu_xO/TiO_2 (Cu^I/Cu^{II} = 1.3).

antibacterial effect (Japanese Industrial Standards, JIS 1702 R). In the assay, test solutions containing bacteriophage Qβ were used to infect *Escherichia coli* (*E. coli*, NBRC 13965), and the bacteriophage concentration was determined from the number of plaque forming units (PFU/mL). As can be seen in Figure 6a, the 0.25% Cu(II)/TiO_2 sample showed only a negligible degree of bacteriophage inactivation in the dark, whereas marked inactivation was observed under visible-light irradiation as a result of an IFCT process.[24] Surprisingly, the 0.25% Cu_xO/TiO_2 (Cu^I/Cu^{II} = 1.3) sample, which contains the same Cu content as the Cu(II)/TiO_2 sample, displayed a 4-log reduction (*i.e.*, 99.99% reduction of phage) after 1 h contact time, even under dark conditions. The activity was further improved under visible-light irradiation, as a 7.5-log reduction of bacteriophage was achieved after 40 min (Figure 6b).

The antipathogenic effects of the samples were further measured using *E. coli* (Gram-negative bacterium, NBRC 3972) and the Gram-positive bacterium *Staphylococcus aureus* (*S. aureus*, NBRC 12732) as model bacteria. A similar trend of inactivation to that for bacteriophage Qβ was found for both *E. coli* and *S. aureus* by the 0.25% Cu_xO/TiO_2 (Cu^I/Cu^{II} = 1.3) sample (Figure 7), demonstrating the high antipathogenic properties of our hybrid Cu_xO/TiO_2 nanocomposites. The activities could be controlled by tuning the ratio of Cu^I/Cu^{II} in the nanocomposites (Figure S10 in the Supporting Information), with a ratio of 1.3 giving the optimum antipathogenic activity. With this optimum composition, photocatalytic oxidation activity under visible-light irradiation was also sufficiently high, as shown in Figure 5. The evaluation of the antipathogenic properties was conducted using a commercial 10 W cylindrical white fluorescent light with a UV-cutoff film at an illuminance of 800 lx, which is commonly used as an indoor lighting source in office buildings, public places, and homes. We can therefore conclude that our Cu_xO/TiO_2 nanocomposite exhibits significant antipathogenic effects under normal indoor conditions.

For comparison, the antiviral properties of bare TiO_2 and $TiO_{2-x}N_x$ were also examined (Figure S11 in the Supporting Information) and were found to have negligible antiviral activity under dark conditions, as well as following visible-light irradiation. We also compared the performance of our 0.25% Cu_xO/TiO_2 nanocomposites with that of 0.25% Cu_2O/TiO_2, which was prepared by physically mixing commercial Cu_2O and TiO_2 powders. We found that the antiviral and antibacterial properties of the Cu_xO/TiO_2 nanocomposite were superior to those of the physically mixed Cu_2O/TiO_2 composite (Figures S11−13 in the Supporting Information), indicating that the few nanometer size of the Cu_xO clusters and their attachment onto the TiO_2 crystals are critical for high antipathogenic activity. We also investigated the antiviral effect of silver (Ag), which is well-known to possess antibacterial activity. Even though Ag exhibited antibacterial activity under dark conditions, no antiviral effects were detected under visible light or in the dark. Taken together, these results indicate that antibacterial agents do not absolutely possess antiviral activity, as the biological structures of bacteria significantly differ from those of viruses with respect to size.[38]

To further explore the antipathogenic effects of the Cu_xO/TiO_2 samples, we investigated the ability of these materials to degrade DNA and proteins, which are essential components of viruses and bacteria. Figure 8a shows the resulting agarose gel electrophoresis patterns after the exposure of supercoiled plasmid

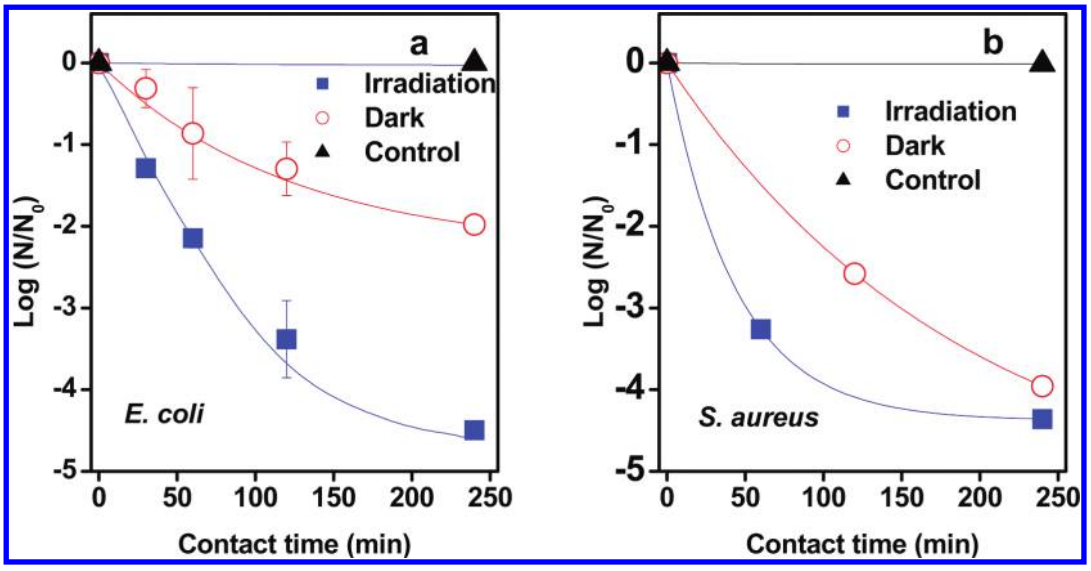

Figure 7. Inactivation of bacteria by 0.25% Cu_xO/TiO_2 (Cu^I/Cu^{II} = 1.3). (a) *E. coli*. (b) *S. aureus*.

pBR322 DNA to the various samples for 2 h under dark conditions. Among the examined samples, bare TiO_2 did not cleave the plasmid DNA; however, conversion of the plasmid DNA from the supercoiled to the open circular form was clearly observed in the systems of the hybrid Cu_xO/TiO_2 nanocomposites. Notably, the degree of degradation increased as the ratio of Cu^I/Cu^{II} in the hybrid Cu_xO/TiO_2 nanocomposites increased. The complete conversion of supercoiled DNA was achieved by the 0.25% Cu_xO/TiO_2 (Cu^I/Cu^{II} = 1.3) sample (Figure 8a; lane 1). We also observed protein degradation by the hybrid Cu_xO/TiO_2 nanocomposites (Figures S14 in the Supporting Information). These experimental observations suggest that the hybrid Cu_xO/TiO_2 nanocomposites are able to destroy the critical biomolecules of bacteria and viruses, leading to their death and inactivation.

Previous studies that investigated the antibacterial and antiviral properties of TiO_2 under UV- or solar-light irradiation[38,40] attributed these activities to direct oxidation by photogenerated holes or reactive radical species, such as ·OH radical, O_2^-, and H_2O_2.[41] The antiviral effects of Cu metal and Cu^{2+} ions under dark conditions in the presence of H_2O_2 were also demonstrated.[42] To understand the effects of copper oxidation state on the antiviral and antibacterial properties, we further studied the antipathogenic effects of CuO and Cu_2O under the same experimental conditions. It is found that Cu_2O was very effective for killing of viruses and bacteria, whereas CuO showed a weak effect on the virus and bacterial inactivation. On the basis of our present results, however, Cu^I species in Cu_xO nanoclusters appear much more effective than Cu metals or Cu^{II} species for enhancing the antiviral and antibacterial effects of TiO_2 photocatalysts. We also confirmed that these activities were not induced by free Cu^+ or Cu^{2+} ions dissolved in water. Together with the finding that Cu^I species are much more effective than metal Cu^0 or Cu^{II} species for the inactivation of bacteria and viruses,[23] our present results indicate that the observed antimicrobial activity under dark conditions is induced by the solid-state Cu_xO nanoclusters with Cu^I. The Cu_xO-mediated mechanism underlying the antivirus phenomenon is currently being investigated biochemically in our laboratory and will be reported elsewhere.

The most important finding of the present study is that this is the first discovery of high antipathogenic activity of TiO_2 hybridized with solid-state Cu_xO nanoclusters, even in dark conditions. Under visible-light irradiation, the electrons in the valence band of TiO_2 are promoted to Cu^{II} species in Cu_xO clusters, representing a form of IFCT, which results in the transformation of Cu^{II} into Cu^I and holes remaining in the valence band.[24] The generated Cu^I can efficiently reduce oxygen molecules *via* a multielectron reduction process and subsequently return to Cu^{II}.[24,27] During visible-light irradiation, the holes generated in the valence band of TiO_2 have strong oxidation power to decompose VOCs, a property that explains the high photooxidation activity of the hybrid Cu_xO/TiO_2 nanocomposites for IPA and acetaldehyde decomposition under this condition. Following irradiation with visible light, holes generated in the valence band of TiO_2 in combination with Cu^I species can also damage the outer membrane, proteins, and nucleic acid (DNA and RNA) of viruses and bacteria, resulting in their death and inactivation. The amount of Cu^I species in the clusters increased by IFCT under visible-light irradiation, and the additional Cu^I species may contribute to the antipathogenic effects of the hybrid Cu_xO/TiO_2 nanocomposites. However, the ratio of Cu^I/Cu^{II} did not markedly change after long-term visible-light irradiation, indicating that the multielectron reduction

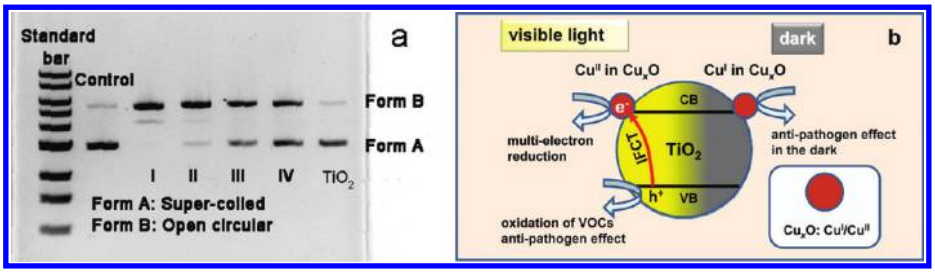

Figure 8. (a) Cleavage of supercoiled plasmid pBR322 DNA by different samples under dark conditions for 2 h. Lanes I, II, III, and IV correspond to the 0.25% Cu_xO/TiO_2 (Cu^I/Cu^{II} = 1.3), 0.25% Cu_xO/TiO_2 (Cu^I/Cu^{II} = 0.2), 0.25% Cu_xO/TiO_2 (Cu^I/Cu^{II} = 0.13), and 0.25% Cu(II)/TiO_2 samples, respectively. (b) Proposed processes of photocatalysis and inactivation of viruses and bacteria under visible-light irradiation and dark conditions.

reaction is catalytic in air with a turnover number greater than 22.[25] These results indicate that both the photocatalytic VOC decomposition and antipathogenic effects in the dark of our generated hybrid Cu_xO/TiO_2 nanocomposites can be sustained for the long-term in indoor environments.

CONCLUSION

In summary, we have succeeded in developing a conceptually different method to deposit nanocluster mixtures (Cu^I and Cu^{II} species) onto TiO_2 surfaces and initially found that both the efficient photocatalytic VOC decomposition and antipathogenic effects in indoor conditions can be achieved in our materials. Furthermore, the detailed structure for our nanoclusters was comprehensively characterized by synchrotron analysis, and the possible mechanism of the multifunctional properties could be elucidated. The balance between Cu^{II} and Cu^I states in Cu_xO is critical to achieve efficient VOC decomposition and antipathogenic activity. It is found that the optimum content of Cu^I in Cu_xO nanoclusters is 56% (Cu^I/Cu^{II} = 1.3). Although the generated Cu_xO/TiO_2 nanocomposite is expected to damage bacteria and viruses, it is formed from titanium and copper, which are not toxic to human health and are naturally abundant and economical elements. Further, our hybrid Cu_xO/TiO_2 nanocomposites are very stable under long-term light irradiation and display multifunctional properties, which make them promising materials for a wide range of applications, including air purification in private housing and public places, such as hospitals, airports, metro stations, and schools, or as air filters, respiratory face masks,[43] and antifungal fabrics,[44] among others. It is also noteworthy that a mass-production process for the Cu_xO/TiO_2 nanocomposites presented here is being developed by Showa Titanium Co., Ltd. (Toyama, Japan), which supports the good performance of Cu_xO/TiO_2 composites for indoor purification applications. More generally, our study indicates a strategic way to develop the nanocomposites for numerous applications.

EXPERIMENTAL SECTION

Synthesis of Cu_xO/TiO_2 Nanocomposite Samples. Commercial TiO_2 (MT-150A, TAYCA Co., rutile phase, 15 nm grain size, 90 m^2/g specific surface area) was used as the starting material. To improve the crystallinity, TiO_2 was annealed at 950 °C for 3 h. The specific surface area was decreased to 3.7 m^2/g. Then, the calcined TiO_2 was treated with 6 M HCl aqueous solution at 90 °C for 3 h under stirring. After filtration, washing, and dry at room temperature, the resulting clear TiO_2 was used to prepare Cu_xO/TiO_2 nanocomposites.

The Cu_xO/TiO_2 nanocomposites were prepared by an impregnation technique. In a typical preparation, one gram of treated TiO_2 was dispersed into 10 mL of $CuCl_2$ solution in a vial reactor. The weight fraction of Cu relative to TiO_2 was set to be 1×10^{-3} to 2×10^{-2}. Under stirring, the sealed vial reactor was incubated at 90 °C for 1 h using a water bath. Then a given amount of NaOH solution and glucose solution were added into the above suspension, which was allowed to react at 90 °C for 1 h. The final products were sufficiently washed and then dried at 110 °C overnight and grounded into powder using an agate mortar. For comparison, the unitary Cu^{II}-nanocluster-grafted TiO_2 was also obtained without any glucose and NaOH and named as Cu(II)/TiO_2.

Sample Characterization. Elemental analyses of the samples were performed using an inductively coupled plasma atomic emission spectrometer (ICP-AES, P-4010, Hitachi) for Ti and Cu. It was found that the total amount of Cu in the prepared samples was nearly equal to the initial concentration used in the preparation. The structural characteristics of the samples were measured by powder X-ray diffraction at room temperature on a Rigaku D/MAX25000 diffractometer with a copper target (λ = 1.54178 Å). The data were collected from $2\theta = 20-70°$ in a step-scan mode (step, 0.02°; counting time, 5s). The microstructures of the samples were investigated by transition electron microscopy on a JEOL JEM 2010 instrument under an acceleration voltage of 200 kV. The specific surface areas of the samples were determined from the nitrogen absorption data at liquid nitrogen temperature using the Barrett–Emmett–Teller technique. The samples were degassed at 200 °C and at a pressure below 100 mTorr for a minimum of 2 h prior to analysis using a Micromeritics VacPrep 061. The absorption spectra of the samples were recorded using a UV-2550 spectrophotometer (Shimadzu). The ionic characteristics and surface composition were studied by X-ray photoelectron spectroscopy (XPS, Perkin-Elmer, 5600). The binding energy data are calibrated with the C 1s signal at 284.6 eV.

Structural features of Cu_xO and the ratio of Cu^I/Cu^{II} in the as-prepared nanocomposites were characterized by X-ray absorption fine structure (XAFS), including X-ray absorption near-edge structure. The XAFS spectra for the Cu K-edge were recorded on beamline 01B01 at SPring-8, which is administered by the Japan Synchrotron Radiation Research Institute (JASRI).[45]

Transmission (standard Cu foil, Cu_2O, CuO, and $Cu(OH)_2$) and fluorescence yield (composites) spectra were acquired using a double-crystal Si(111) monochromator, ion chambers, and a 19-element germanium solid-state detector equipped with a nickel filter. The XAFS data were analyzed using the REX2000 (Rigaku Corporation) and FEFF programs.[46] Cu_2O and $Cu(OH)_2$ mixtures were used as the standard specimen to extract experimental EXAFS parameters to determine the ratio of Cu^I/Cu^{II} in the hybrid Cu_xO/TiO_2 nanocomposite.

Acknowledgment. This work was performed under the management of the Project To Create Photocatalyst Industry for Recycling-Oriented Society supported by the New Energy and Industrial Technology Development Organization (NEDO) in Japan. The synchrotron radiation experiments were performed at the BL14B2 of SPring-8 with the approval of the Japan Synchrotron Radiation Research Institute (JASRI) (Proposal No. 2010B1010).

Supporting Information Available: Detailed information of photocatalytic, antiviral, and antibacterial data, protein and DNA degradation experiments, UV−visible spectra of 0.25% Cu_xO/TiO_2 nanocomposites with different Cu^I/Cu^{II} ratios, XPS and XANES analysis in detail, EDX point analysis, irradiation light source, comparative studies of CO_2 generation over Cu_xO/TiO_2 nanocomposites with different Cu content under visible-light irradiation, comparative studies of CO_2 generation over 0.25% Cu_xO/TiO_2 nanocomposites with various ratios of Cu^I/Cu^{II} under visible-light irradiation, stability of Cu_xO/TiO_2 sample for the photocatalysis, calculated quantum efficiencies and CO_2 generation rate, comparative studies of inactivation of bacteriophage Qβ on 0.25% Cu_xO/TiO_2 nanocomposites with various ratios of Cu^I/Cu^{II}, antipathogen effects of $TiO_{2-x}N_x$, comparative studies of antipathogen effects of 0.25%Cu_xO/TiO_2 nanocomposites and 0.25% Cu_2O/TiO_2 physical mixture, and degradation of protein on 0.25% Cu_2O/TiO_2 nanocomposites. This information is available free of charge *via* the Internet at http://pubs.acs.org.

REFERENCES AND NOTES

1. Spengler, J. D.; Sexton, K. Indoor Air Pollution: A Public Health Perspective. *Science* **1983**, *221*, 9–17.
2. Klepeis, N. E.; Nelson, W. C.; Ott, W. R.; Robinson, J. P.; Tsang, A. M.; Switzer, P.; Behar, J. V.; Hern, S. C.; Engelmann, W. H. The National Human Activity Pattern Survey (NHAPS): a resource for assessing exposure to environmental pollutants. *J. Expo. Anal. Environ. Epidemiol.* **2001**, *11*, 231–252.
3. Harada, K.; Hasegawa, A.; Wei, C. N.; Minamoto, K.; Noguchi, Y. N.; Hara, K.; Matsushita, O.; Noda, K.; Ueda, A. A Review of Indoor Air Pollution and Health Problems from the Viewpoint of Environmental Hygiene: Focusing on the Studies of Indoor Air Environment in Japan Compared to Those of Foreign Countries. *J. Health Sci.* **2010**, *56*, 488–501.
4. Morens, D. M.; Folkers, G. K.; Fauci, A. S. The Challenge of Emerging and Re-emerging Infectious Diseases. *Nature* **2004**, *430*, 242–249.
5. Jones, K. E.; Patel, N. G.; Levy, M. A.; Storeygard, A.; Balk, D.; Gittleman, J. L.; Daszak, P. Global Trends in Emerging Infectious Diseases. *Nature* **2008**, *451*, 990–993.
6. Fujishima, A.; Zhang, X.; Tryk, A. D. TiO_2 Photocatalysis and Related Surface Phenomena. *Surf. Sci. Rep.* **2008**, *63*, 515–582.
7. Hoffmann, M. R.; Martin, S. T.; Choi, W.; Bahnemann, D. W. Environmental Applications of Semiconductor Photocatalysis. *Chem. Rev.* **1995**, *95*, 69–96.
8. Linsebigler, A. L.; Lu, G. Q.; Yates, J. T. Photocatalysis on TiO_2 Surfaces: Principles, Mechanisms, and Selected Results. *Chem. Rev.* **1995**, *95*, 735–758.
9. Miyauchi, M.; Nakajima, A.; Hashimoto, K.; Watanabe, T. A Highly Hydrophilic Thin Film Under 1 $\mu W/cm^2$ UV Illumination. *Adv. Mater.* **2000**, *12*, 1923−1927.
10. Choi, W. Y.; Termin, A.; Hoffmann, M. R. The Role of Metal Ion Dopants in Quantum-Sized TiO_2: Correlation between Photoreactivity and Charge Carrier Recombination Dynamics. *J. Phys. Chem.* **1994**, *98*, 13669–13679.
11. Chen, X.; Mao, S. S. Titanium Dioxide Nanomaterials: Synthesis, Properties, Modifications, and Applications. *Chem. Rev.* **2007**, *107*, 2891–2959.
12. Yamashita, H.; Harada, M.; Misaka, J.; Takeuchi, M.; Ikeue, K.; Anpo, M. Degradation of Propanol Diluted in Water Under Visible Light Irradiation Using Metal Ion-Implanted Titanium Dioxide Photocatalysts. *J. Photochem. Photobiol. A* **2002**, *148*, 257–261.
13. Asahi, R.; Morikawa, T.; Ohwaki, T.; Aoki, K.; Taga, Y. Visible-Light Photocatalysis in Nitrogen-Doped Titanium Oxides. *Science* **2001**, *293*, 269–271.
14. Khan, S. U. M.; Al-Shahry, M.; Ingler, W. B. Efficient Photochemical Water Splitting by a Chemically Modified n-TiO_2. *Science* **2002**, *297*, 2243–2245.
15. Sakthivel, S.; Kisch, H. Daylight Photocatalysis by Carbon-Modified Titanium Dioxide. *Angew. Chem., Int. Ed.* **2003**, *42*, 4908–4911.
16. Kamat, P. V.; Meisel, D. Nanoparticles in Advanced Oxidation Processes. *Curr. Opin. Colloid Interface Sci.* **2002**, *7*, 282–287.
17. Irie, H.; Watanabe, Y.; Hashimoto, K. Nitrogen-Concentration Dependence on Photocatalytic Activity of $TiO_{2-x}N_x$ Powders. *J. Phys. Chem. B* **2003**, *107*, 5483–5486.
18. Elahifard, M. R.; Rahimnejad, S.; Haghighi, S.; Gholami, M. R. Apatite-Coated Ag/AgBr/TiO_2 Visible-Light Photocatalyst for Destruction of Bacteria. *J. Am. Chem. Soc.* **2007**, *129*, 9552–9553.
19. Barreca, D.; Carraro, G.; Gasparotto, A. Cu_xO-TiO_2 Composites (x = 1, 2) Studied by X-ray Photoelectron Spectroscopy. *Surf. Sci. Spectra* **2009**, *16*, 1–12.
20. Barreca, D.; Carraro, G.; Gombac, V.; Gasparotto, A.; Maccato, C.; Fornasiero, P.; Tondello, E. Supported Metal Oxide Nanosystems for Hydrogen Photogeneration: Quo Vadis? *Adv. Funct. Mater.* **2011**, *21*, 2611–2623.
21. Barreca, D.; Carraro, G.; Gasparotto, A.; Maccato, C.; Lebedev, O. I.; Parfenova, A.; Turner, S.; Tondello, E.; Van Tendeloo, G. Tailored Vapor-Phase Growth of Cu_xO-TiO_2 (x = 1, 2) Nanomaterials Decorated with Au Particles. *Langmuir* **2011**, *27*, 6409–6417.
22. Barreca, D.; Carraro, G.; Comini, E.; Gasparotto, A.; Maccato, C.; Sada, C.; Sberveglieri, G.; Tondello, E. Novel Synthesis and Gas Sensing Performances of CuO-TiO_2 Nanocomposites Functionalized with Au Nanoparticles. *J. Phys. Chem. C* **2011**, *115*, 10510–10517.
23. Hashimot, K.; Sunada, K.; Miyauchi, M.; Qiu, X. Q.; Yoshinobu, K.; Hitoshi, I.; Ryuichi, N.; Jitsuo, K.; Yao, Y. Y. PCT patent application, PCT/JP2010/073087.
24. Irie, H.; Miura, S.; Kamiya, K.; Hashimoto, K. Efficient Visible Light-Sensitive Photocatalysts: Grafting Cu(II) Ions onto TiO_2 and WO_3 Photocatalysts. *Chem. Phys. Lett.* **2008**, *457*, 202–205.
25. Yu, H. G.; Irie, H.; Hashimoto, K. Conduction Band Energy Level Control of Titanium Dioxide: Toward an Efficient Visible-Light-Sensitive Photocatalyst. *J. Am. Chem. Soc.* **2010**, *132*, 6898–6899.
26. Yu, H. G.; Irie, H.; Shimodaira, Y.; Hosogi, Y.; Kuroda, Y.; Miyauchi, M.; Hashimoto, K. An Efficient Visible-Light-Sensitive Fe(III)-Grafted TiO_2 Photocatalyst. *J. Phys. Chem. C* **2010**, *114*, 16481–16487.
27. Qiu, X. Q.; Miyauchi, M.; Yu, H. G.; Irie, H.; Hashimoto, K. Visible-Light-Driven Cu(II)-$(Sr_{1-y}Na_y)(Ti_{1-x}Mo_x)O_3$ Photocatalysts Based on Conduction Band Control and Surface Ion Modification. *J. Am. Chem. Soc.* **2010**, *132*, 15259–15267.
28. Irie, H.; Kamiya, K.; Shibanuma, T.; Miura, S.; Trky, D. A.; Yokoyama, T.; Hashimoto, K. Visible Light-Sensitive Cu(II)-Grafted TiO_2 Photocatalysts: Activities and X-ray Absorption Fine Structure Analyses. *J. Phys. Chem. C* **2009**, *113*, 10761–10766.
29. Dias, N. L. Adsorption of Cu(II) and Co(II) Complexes on a Silica Gel Surface Chemically Modified with 2-Mercaptoimidazole. *Mikrochim. Acta* **1999**, *130*, 233–240.
30. Banerjee, S.; Chakravorty, D. Optical Absorption by Nanoparticles of Cu_2O. *Europhys. Lett.* **2000**, *52*, 468–473.
31. Oku, M.; Wagatsuma, K.; Kohiki, S. Ti 2p and Ti 3p X-Ray Photoelectron Spectra for TiO_2, $SrTiO_3$ and $BaTiO_3$. *Phys. Chem. Chem. Phys.* **1999**, *1*, 5327–5331.

32. Huang, L.; Peng, F.; Ohuchi, F. S. "*In Situ*" XPS Study of Band Structures at Cu_2O/TiO_2 Heterojunctions Interface. *Surf. Sci.* **2009**, *603*, 2825–2834.
33. Li, G. H.; Dimitrijevic, N. M.; Chen, L.; Rajh, T.; Gray, K. A. Role of Surface/Interfacial Cu^{2+} Sites in the Photocatalytic Activity of Coupled $CuO-TiO_2$ Nanocomposites. *J. Phys. Chem. C* **2008**, *112*, 19040–19044.
34. Kau, L. S.; Spira-Solomon, D. J.; Penner-Hahn, J. E.; Hodgson, K. O.; Solomon, E. I. X-ray Absorption Edge Determination of the Oxidation State and Coordination Number of Copper. Application to the Type 3 Site in Rhus Vernicifera Laccase and its Reaction with Oxygen. *J. Am. Chem. Soc.* **1987**, *109*, 6433–6442.
35. Maurizio, C.; d'Acapito, F.; Benfatto, M.; Mobilio, S.; Cattaruzza, E.; Gonella, F. Local Coordination Geometry Around Cu^{+} and Cu^{2+} Ions in Silicate Glasses: An X-ray Absorption Near Edge Structure Investigation. *Eur. Phys. J. B* **2000**, *14*, 211–216.
36. Wolkoff, P.; Nielsen, G. D. Organic Compounds in Indoor Air - Their Relevance for Perceived Indoor Air Quality?. *Atmos. Environ.* **2001**, *35*, 4407–4417.
37. Ohko, Y.; Hashimoto, K.; Fujishima, A. Kinetics of Photocatalytic Reactions Under Extremely Low-Intensity UV Illumination on Titanium Dioxide Thin Films. *J. Phys. Chem. A* **1997**, *101*, 8057–8062.
38. Palese, P.; Young, J. F. Variation of Influenza A, B, and C Viruses. *Science* **1982**, *215*, 1468–1474.
39. Wei, C.; Lin, W. Y.; Zainal, Z.; Williams, N. E.; Zhu, K.; Kruzic, A. P.; Smith, R. L.; Rajeshwar, K. Bactericidal Activity of TiO_2 Photocatalyst in Aqueous Media: Toward A Solar-Assisted Water Disinfection System. *Environ. Sci. Technol.* **1994**, *28*, 934–938.
40. Cho, M.; Chung, H. M.; Choi, W. Y.; Yoon, J. Y. Different Inactivation Behaviors of MS-2 Phage and *Escherichia coli* in TiO_2 Photocatalytic Disinfection. *Appl. Environ. Micron.* **2005**, *71*, 270–275.
41. Sunada, K.; Watanabe, T.; Hashimoto, K. Studies on Photokilling of Bacteria on TiO_2 Thin Film. *J. Photochem. Photobiol. A* **2003**, *156*, 227–233.
42. Sagripanti, J. L.; Routson, L. B.; Lytle, C. D. Virus Inactivation by Copper or Iron Ions Alone and in the Presence of Peroxide Appl. *Environ Microbiol.* **1993**, *59*, 4374–4376.
43. Borkow, G.; Zhou, S. S.; Page, T.; Gabbay A Novel Anti-Influenza Copper Oxide Containing Respiratory Face Mask. *J. Plos One* **2010**, *5*, e11295.
44. Borkow, G.; Zatcoff, R. C.; Gabbay, J. Reducing the Risk of Skin Pathologies in Diabetics by Using Copper Impregnated Socks. *Med. Hypotheses* **2009**, *73*, 883–886.
45. Uruga, T.; Tanida, H.; Yoneda, Y.; Takeshita, K.; Emura, S.; Takahashi, M.; Harada, M.; Nishihata, Y.; Kubozono, Y.; Tanaka, T.; *et al.* The XAFS Beamline BL01B1 at SPring-8. *Synchrotron Radiat* **1999**, *6*, 143–145.
46. Stern, E. A.; Newville, M.; Ravel, B.; Yacoby, Y.; Haskel, D. The UWXAFS Analysis Package: Philosophy and Details. *Phys. B (Amsterdam, Neth.)* **1995**, *209*, 117–120.